The Astrophysical Journal, 849:85 (8pp), 2017 November 10 https://doi.org/10.3847/1538-4357/aa8e98

SFADI: The Speckle-free Angular Differential Imaging Method

Gianluca Li Causi[1,2,3], Marco Stangalini[2,3], Simone Antoniucci[2,3], Fernando Pedichini[2,3], Massimiliano Mattioli[2,3], and Vincenzo Testa[2,3]
[1] INAF Istituto di Astrofisica e Planetologia Spaziali—Via Fosso del Cavaliere 100, Roma, Italy; gianluca.licausi@oa-roma.inaf.it
[2] INAF Osservatorio Astronomico di Roma—Via Frascati 33, I-00078, Monte Porzio Catone (RM), Italy
[3] ADONI Adaptive Optics National Lab of Italy
Received 2017 July 25; accepted 2017 September 5; published 2017 November 6

Abstract

We present a new processing technique that significantly improves the angular differential imaging method (ADI). Its context of application is that of high-contrast imaging of faint objects nearby bright stars in observations obtained with extreme adaptive optics (EXAO) systems. This technique, named "SFADI" for "Speckle-Free ADI," improves the achievable contrast by means of speckles identification and suppression. This is possible in very high cadence data, which freeze the atmospheric evolution. Here we present simulations in which synthetic planets are injected into a real millisecond frame rate sequence, acquired at the LBT telescope at a visible wavelength, and show that this technique can deliver a low and uniform background, allowing for unambiguous detection of 10^{-5} contrast planets, from 100 to 300 mas separations, under poor and highly variable seeing conditions (0.8 to 1.5 arcsec FWHM) and in only 20 minutes of acquisition. A comparison with a standard ADI approach shows that the contrast limit is improved by a factor of 5. We extensively discuss the SFADI dependence on the various parameters like the speckle identification threshold, frame integration time, and number of frames, as well as its ability to provide high-contrast imaging for extended sources and also to work with fast acquisitions.

Key words: instrumentation: adaptive optics – methods: data analysis – techniques: high angular resolution

1. Introduction

Direct imaging of exoplanets (see, for example, Males et al. 2014a; Bonnefoy 2015; Currie 2015; Hardy et al. 2015 to mention a few) has recently become possible thanks to both technological advances of extreme adaptive optics (EXAO) systems (see, for instance, Beuzit et al. 2006; Cavarroc et al. 2006; Macintosh et al. 2008; Esposito et al. 2010; Davies & Kasper 2012; Kasper 2012; Bailey et al. 2014; Close et al. 2014; Macintosh et al. 2014; Pedichini et al. 2017), and the introduction of high efficiency post-processing techniques like angular differential imaging (ADI; Marois et al. 2006; Lafrenière et al. 2007), Karhunen-Loève image decomposition (KL; Soummer et al. 2012), or principal component analysis (PCA; Amara & Quanz 2012). These methods allow the post-facto reduction of the stray light from the central star on the surrounding areas, with the aim of increasing the contrast and of revealing nearby sources, at angular separations of the order of a few hundreds of milliarcseconds. Indeed, the combination of EXAO and post-facto techniques yields impressive results in terms of faint source detectability (Males et al. 2014b; Pedichini et al. 2017). While EXAO is by far the most important ingredient to boost the image contrast, ADI and other post-facto techniques are fundamental to get the most out of the data. The main idea behind them relies on the subtraction of the point-spread function (PSF) of the central object in order to increase the contrast in the surrounding region. This is done by estimating the PSF itself. This task is usually accomplished by considering the median PSF, estimated through an observation composed of a temporal sequence of images, and by subtracting it from each frame of the sequence. It is worth noting that this PSF estimate may suffer from the intrinsic rapid variations of the seeing conditions. In other words, the estimated PSF may not be the ideal model at each instant, especially in the presence of highly varying seeing conditions, and this may result in suboptimal results.

The adoption of very fast acquisition systems, providing exposures of one or a few milliseconds, can freeze the atmospheric turbulence evolution, and offer a solution to this shortcoming, as originally proposed by Labeyrie (1995). Very recently, Pedichini et al. (2017) and Stangalini et al. (2017) have highlighted the importance of fast cadence in reducing residual jitter and in the application of post-facto techniques, by exploiting new 1 ms cadence data acquired by the SHARK-VIS Forerunner experiment at LBT.

Here we present a new post-facto contrast enhancing method optimized for very high cadence imagers like the SHARK-VIS Forerunner. This technique is based on the identification and removal of residual speckles in millisecond exposure images, and can be seen as a "speckle-free" extension of the standard ADI technique. For this reason, we refer to this technique as to "Speckle-Free ADI" (SFADI).

2. Data Set

The data set used in this work consists of a 20-minute acquisition of 1.2×10^6 sequential 1 ms exposure images of the target Gliese 777 (see the left panel of Figure 1), acquired with the SHARK-VIS Forerunner experiment at LBT on 2015 June 4. The SHARK-VIS Forerunner experiment consisted of a set of short test observations performed at the LBT telescope to verify its EXAO system performance at visible wavelengths ($600 < \lambda < 700$ nm) between 2015 February and June (Pedichini et al. 2017). The experimental setup is minimal and composed of only two optical elements before the detector: one divergent lens to get a super sampling (twice the Nyquist limit) of the PSF and a 40 nm FWHM filter centered at 630 nm. The AO control and wavefront sensing is left to the LBTI Adaptive Optics subsystem (FLAO) fed through a 50% beam

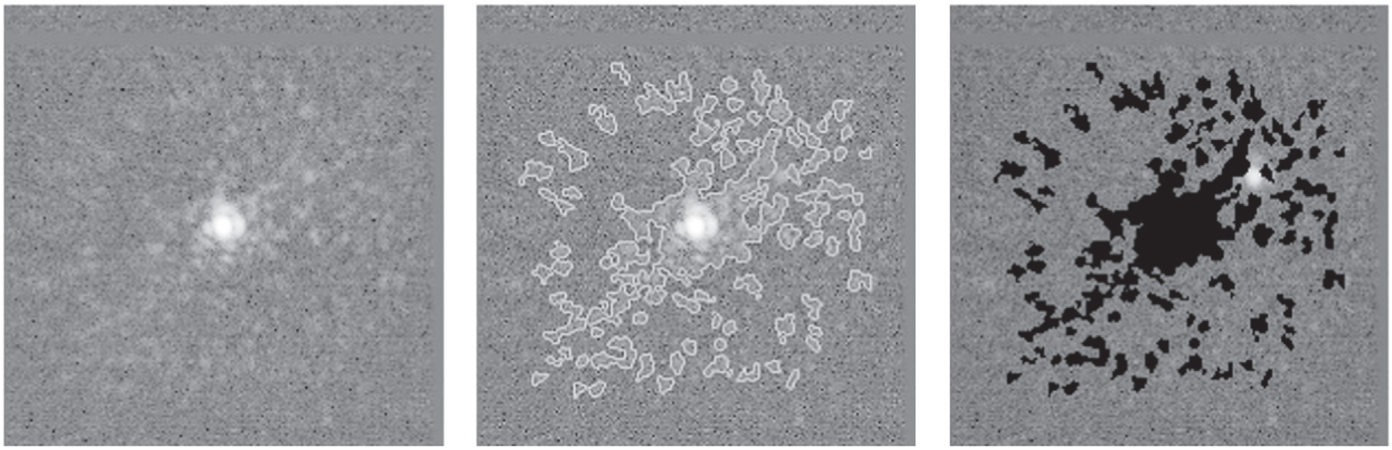

Figure 1. SFADI concept: the speckles in each original frame of the acquisition sequence (left) are identified by the SWAMIS feature recognition code (center), and masked out to leave only the starlight-unaffected background regions (right), where possible sources (we injected here a bright 10^{-1} contrast planet for greater clarity) can be imaged with no light pollution from the central star.

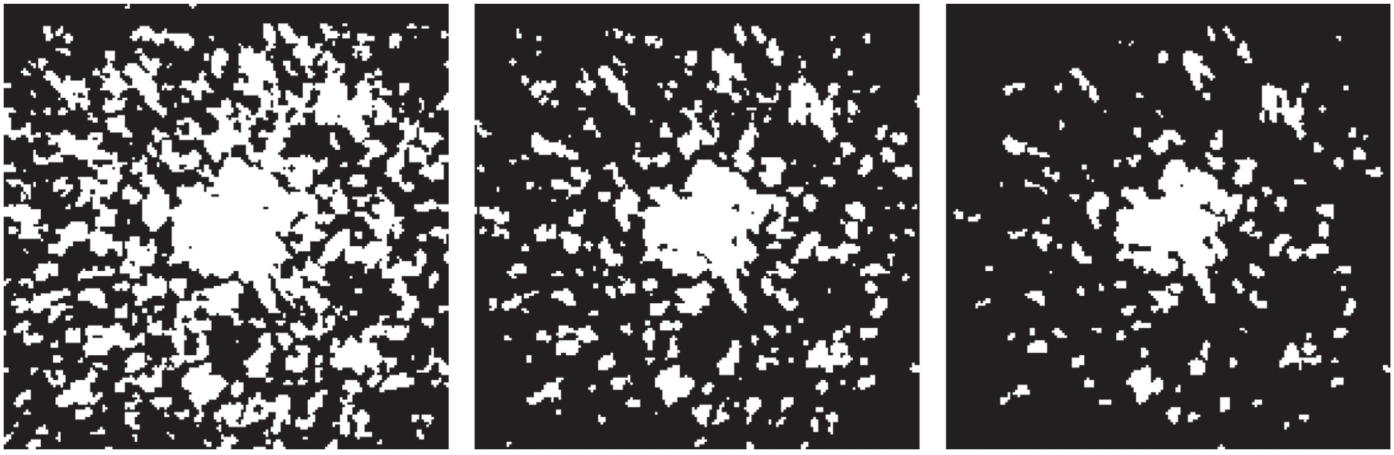

Figure 2. Speckle identification obtained by the SWAMIS code with a threshold of 2, 3, and 4 ADU (from left to right, respectively).

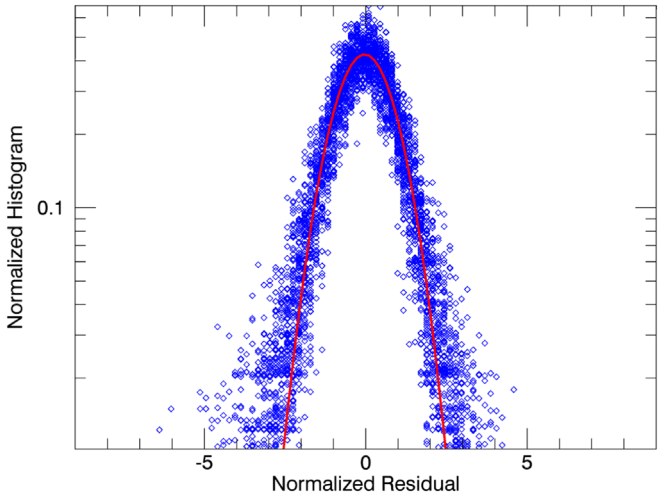

Figure 3. Gaussian distribution of pixel values in the sky-aligned frames of the SFADI, for 100 samples at 150 mas distance from the star. Gaussian fit is overplotted in red.

splitter. The pixel scale is set at 3.73 mas, and the imager is a Zyla sCMOS camera manufactured by Andor Inc.[4] During the acquisition, the LBTI-AO system (Esposito et al. 2010) was correcting 500 modes in the closed loop. The AO frequency was 990 Hz with a loop delay of 3 ms. In these conditions, the closed loop 0 db bandwidth is 59 Hz. The seeing FWHM was in the range of 0.8 to 1.5 arcsec, and no field de-rotator is employed on the mount to correct for sky rotation, in order to implement an ADI-like approach to the data reduction. For more information about the data set and the acquisition system, we refer the reader to Pedichini et al. (2017) and Stangalini et al. (2017).

3. The Standard ADI and the New SFADI Method

The so-called ADI technique (Marois et al. 2006) is based on a three-step concept: (i) all the frames of the acquisition sequence are co-registered (through FFT phase correlation in our case), (ii) the median of all the frames is computed, and used as the PSF model that is subtracted from each single frame of the sequence, and (iii) the PSF-subtracted residuals are de-rotated to compensate for field rotation, and median-combined to obtain the resulting image, mostly free from the contribution of the bright star PSF.

If the PSF did not vary among frames, the ADI would lead to a complete subtraction of the starlight, because the median PSF across the frames would be a good representation of the instant PSF at all times. In practice, however, as shown in Pedichini et al. (2017), the seeing evolution can be highly variable throughout the observation, so that the median of the frames

[4] http://www.andor.com/

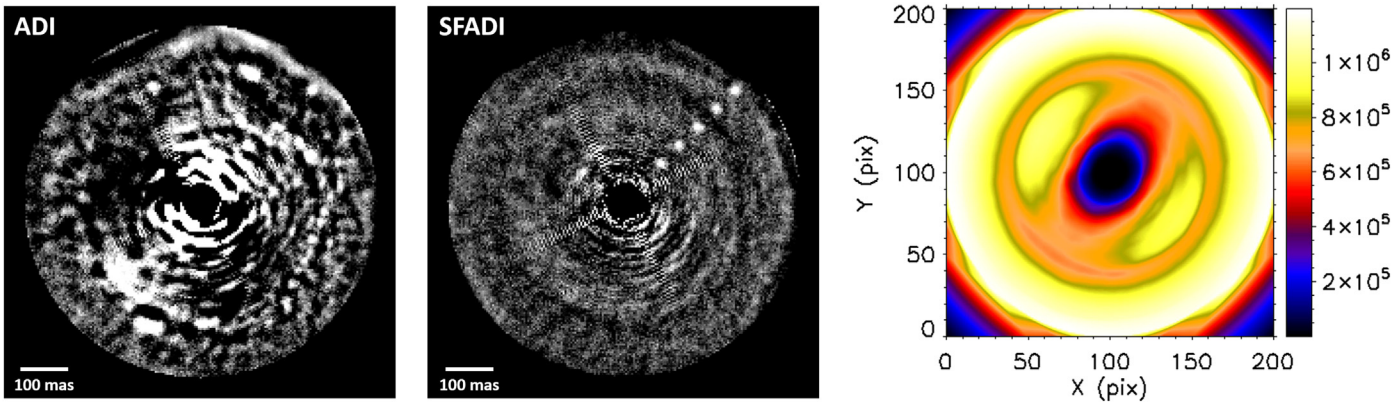

Figure 4. ADI and SFADI results, for the full 1.2×10^6 frames sequence described in the text, in which five synthetic 2×10^{-5} contrast planets at 100 to 300 mas separations were injected. The ADI result is shown in the left panel: only the planet at 300 mas is visible, but it is impossible to distinguish it, if previously unknown, because its flux is comparable to the residual features in the background. The SFADI result is shown in the central panel using the same grayscale: all the planets are clearly distinguishable over a much lower and uniform residual background. Regions closer than 35 mas and outside 340 mas, which contain the strongest artifacts, have been masked for clarity. The right panel depicts the map of the number of combined frames per pixel in the SFADI combination.

does not match the instantaneous PSF of any frame, producing strong residuals in the ADI result, which limits the achievable image contrast.

The SFADI method overcomes some of the above limitations through the full exploitation of the fast (1 ms) cadence of the data.

In fact, the frame by frame PSF evolution is due to the rapid variation of the adaptive optics residuals, which appears as a pattern of speckles changing shape with a timescale of less than 10 ms, at visible wavelengths, as shown in Stangalini et al. (2017). Hence, if the frame rate is fast enough, i.e., of the order of a few milliseconds, all the speckles are basically frozen (see Section 3.1) and they appear as compact sharp features in each frame, not smoothed by their fast movement (left panel in Figure 1). In this case, a suitable image recognition algorithm can be employed to identify and suppress them in each frame. As the star light is, in practice, completely contained in the speckles, the background pixels in between them will ideally contain no star light at all. Figure 1 qualitatively illustrates this concept. Thus, if we exclusively use these background pixels in a standard ADI processing, we expect to have no speckle-induced artifacts in the final result, as shown in the second panel of Figure 4, because we only combine speckle-free regions from each frame.

3.1. Speckle Identification

The first step of our method is the identification of the speckles in each single frame. This step is accomplished by using the SWAMIS code (DeForest et al. 2007). This code was originally written for the identification and tracking of small-scale magnetic elements in the solar photosphere (Lamb et al. 2008, 2010, 2013), a task conceptually similar to that of the identification of faint speckles in AO data (Stangalini 2014; Stangalini et al. 2015). In short, the code uses a double-threshold clump identification scheme that allows the labeling of small-scale features. While the higher threshold is not necessary for our purpose and can be set to an arbitrarily high value, the second lower threshold allows us to isolate clusters of pixels above the noise, and is typically set at 2–3σ, where σ is the standard deviation of the noise. The σ of the noise distribution of our data set, computed in a region 300 mas away from the central source, is 2.3 ADU.

In addition to this threshold, another stringent constraint is used to reject noise. Indeed, only clumps with a size larger than the resolution angle are selected (i.e., not smaller than the average FWHM of $\sim$4 pixels of the PSF core in our data set). This implies that only structures with a spatial scale of the order of the PSF core are identified, thus ruling out the possibility of including noise features and also allowing identification of very faint speckles next to the noise level.

This code was already used by Stangalini et al. (2017) on exactly the same data to study the statistics of speckles in AO images at visible wavelengths. The main conclusions of this analysis were that 90% of the AO residual speckles have a lifetime shorter than 5 ms. This means that, at least at visible wavelengths, a very fast cadence of the order of 1 KHz is required for the succesful application of the SFADI technique or any other deconvolution method (e.g., Jefferies & Hart 2011) that relies on the freezing of the atmospheric turbulence evolution.

For further details on the application of the SWAMIS code for the identification of AO residual speckles, we refer the reader to Stangalini et al. (2017).

The outputs of the SWAMIS code are binary masks that identify clusters of pixels belonging to the same speckle. In Figure 2, we show examples of such identification for different thresholds (i.e., 2, 3, and 4 ADU): the lower the intensity threshold the larger the number of speckles identified outside the central core of the PSF. In contrast, larger thresholds allow us to isolate different speckles in the PSF core, which otherwise would appear as a single extended feature.

3.2. Frame Combination

After identification of speckles in all frames, we compute the median background across the whole sequence, like one usually does in the ADI, but excluding the masked pixels. Then we take this median background as representative of the instant inter-speckle background at all times, and subtract it from each frame, still excluding the pixels belonging to identified speckles. Finally, we perform the numerical derotation of these background-subtracted and masked frames, thus obtaining the stack of sky-aligned frames to be combined in the resulting image.

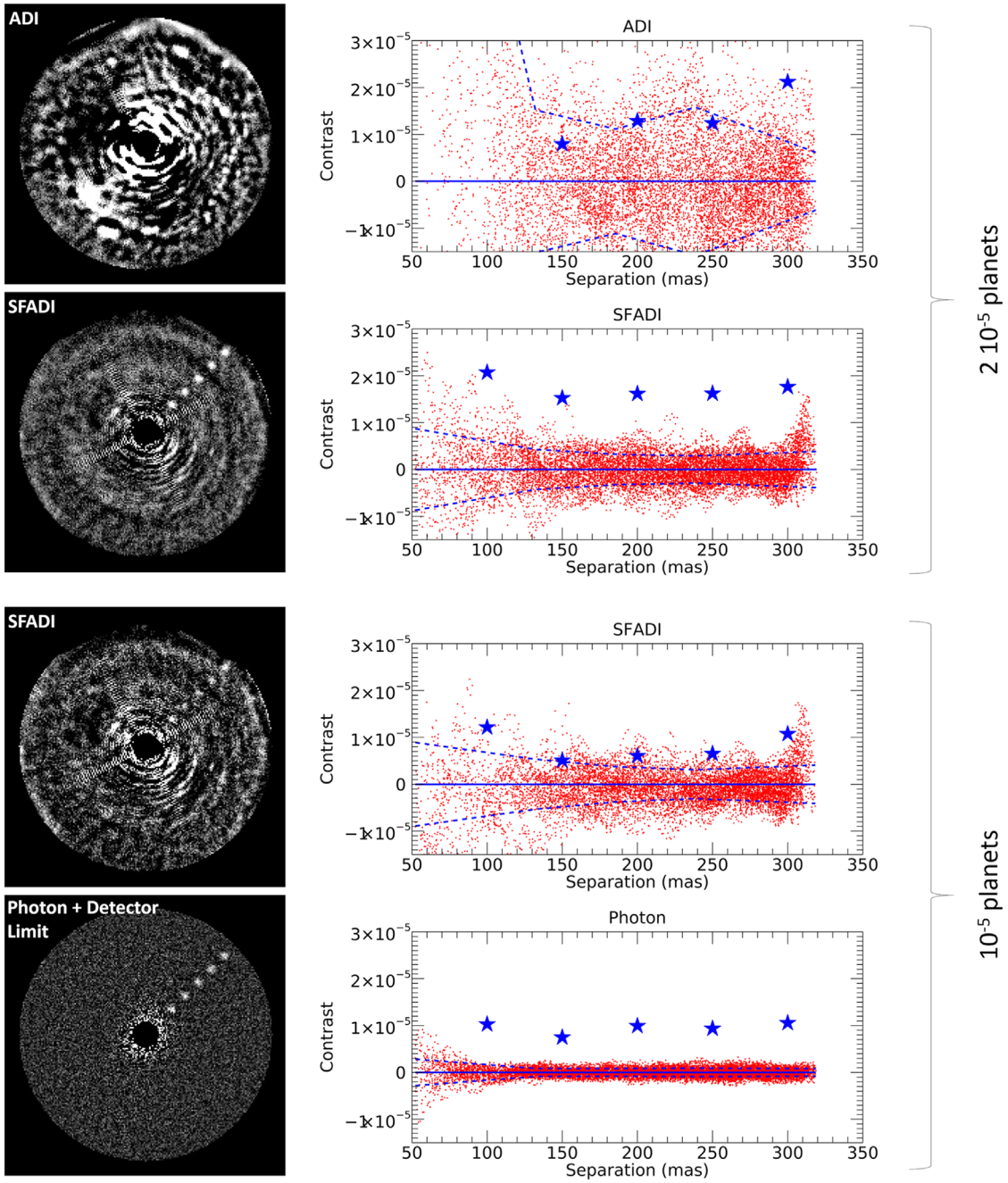

Figure 5. Planet detection performance for 2×10^{-5} contrast planets with ADI (top) and SFADI (second row): planets' aperture photometries (blue star symbols) are compared to background aperture photometry at each pixel location (red dots), whose standard deviation is indicated by the blue dashed lines as a function of separation from the central star. Third row: same analysis for 10^{-5} contrast planets. The theoretical photon limit, with 10^{-5} contrast planets, is shown in the bottom row, for comparison.

In the standard ADI, this combination of the aligned frames must be unavoidably computed through a median operator, because outlying pixel values are present wherever the median PSF differs from the instant PSF. This usually leads to artifacts in the combined result as shown in the left panel of Figure 4.

In contrast, the distribution of pixel values in the sky-aligned frames of the SFADI is Gaussian (Figure 3) because no outliers are present in the inter-speckle background. Such a situation allows us to combine the sky-aligned frames of the SFADI by means of a simple arithmetic average, which delivers a very uniform and artifact-free background in the resulting image, as we show in the central panel of Figure 4.

This also yields a significant gain in computation time, as we adopt a straightforward running average, only slightly modified to exclude the masked pixels, which is much faster and less memory consuming than the median operator.

Figure 4 shows a direct comparison of the ADI and the SFADI result for our full 1.2×10^6 frames sequence, in which we injected five planets 2×10^{-5} times fainter than the star, with separations of 50 mas from 100 to 300 mas off-axis, and

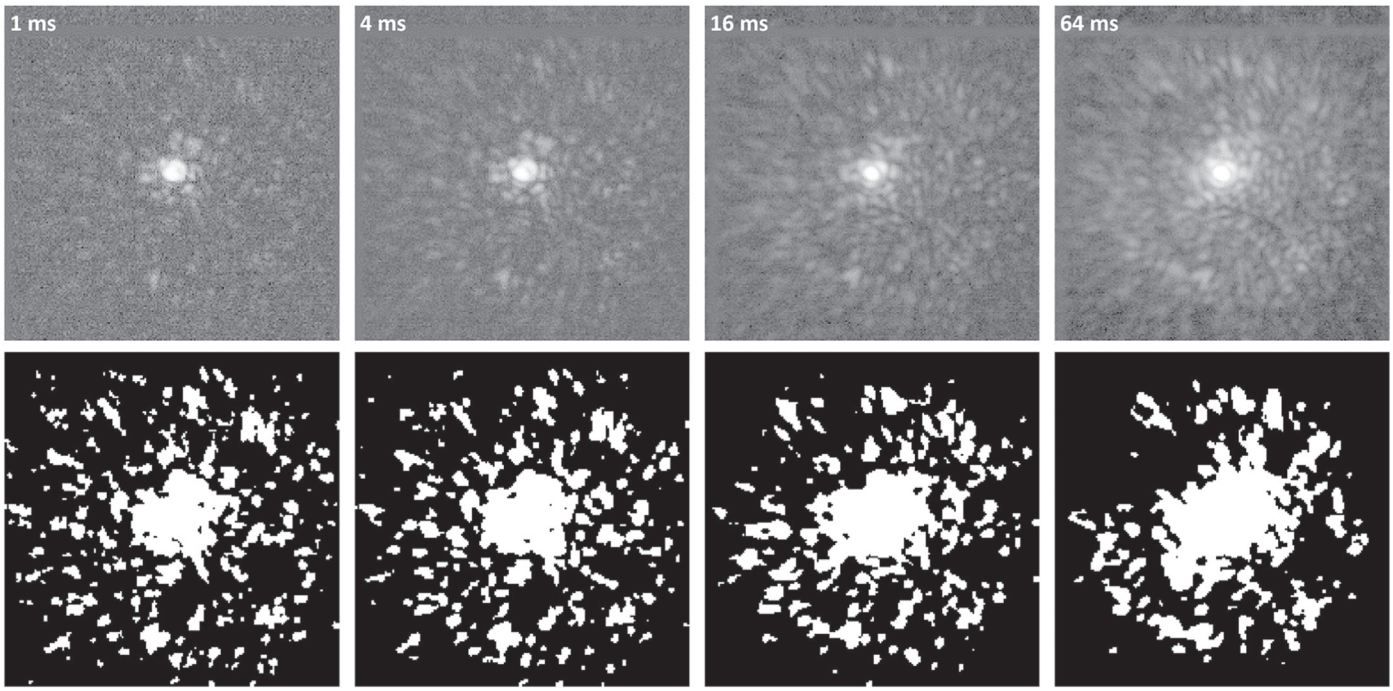

Figure 6. Speckles (top) and speckle recognition masks (bottom) for frame exposures of 1, 4, 16, and 64 ms (from left to right respectively).

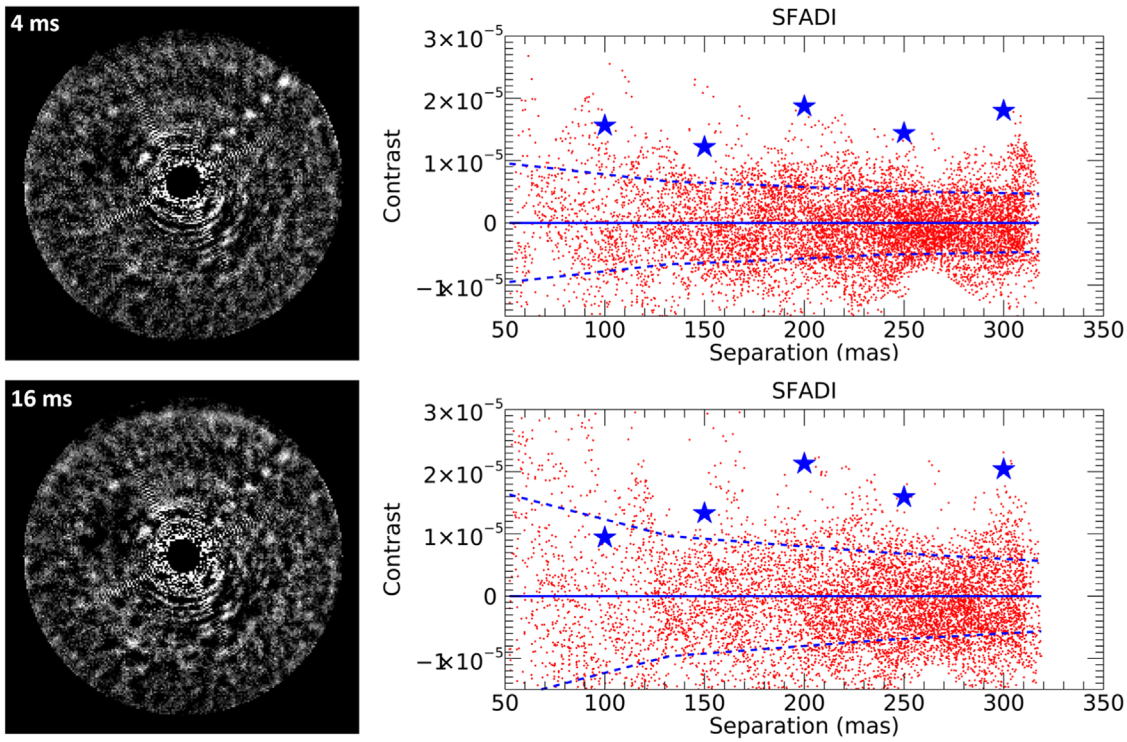

Figure 7. SFADI results for frame exposures of 4 ms and 16 ms (top and bottom respectively), to be compared with the 1 ms case in the second panel of Figure 5.

aligned at 45 deg, i.e., along the direction where the ADI residual is found to be worse. In the same figure, we also show the map of the number of combined frames per pixel (right panel), as in the SFADI a different number of sky-aligned frames are effectively combined for each pixel of the final image.

For this figure, we injected planets fainter than the ADI detection limit of 5×10^{-5} achieved by Pedichini et al. (2017), using the same data. The improvement over the standard ADI method is evident. This will be quantitatively characterized in the following section.

3.3. SFADI Characterization

In this section, we present a quantitative comparison of the SFADI performances with respect to a standard ADI and to the photon limit, for a different number of frames and different frame integration times.

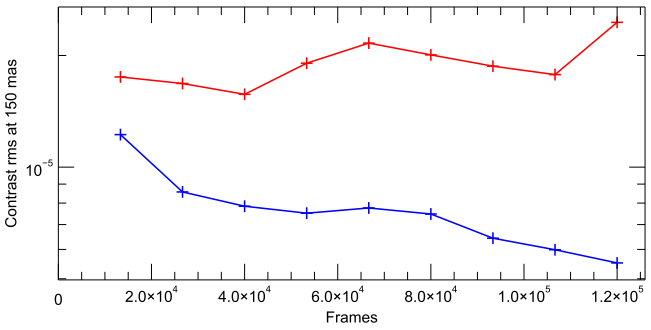

Figure 8. ADI (red) and SFADI (blue) contrast rms of background residuals photometry as a function of the number of frames of the acquisition sequence. Note that a subset of 1 frame every 10 has been used here to speed up the computation time.

The metric that we adopted to perform this comparison relies on the ratio of the aperture photometry at injected planet positions to the standard deviation of the same aperture photometry at each pixel location in the background.

Both the ADI and SFADI combined images have been processed, before photometry, by subtracting a 3 FWHM box-median filtering and a 360 degrees angular median, in order to flatten the large-scale background variations.

Top and second row in Figure 5 show the planet's photometry (stars) compared with the background photometry (red dots). It is shown that in the ADI the 2×10^{-5} planets lie at only 1σ above the background, while in the SFADI they lie at 3σ above background. The third row of the same figure shows that even a planet contrast as low as 1×10^{-5} is still well detectable at all distances with the SFADI method. It is worth noting that an advanced detection algorithm would recognize planets even fainter than these, as it would also recognize the point sources against the background residuals, which have a very different shape.

Finally, in the bottom row of Figure 5, we show the same analysis applied to a numerical simulation, which takes into account the actual number of aligned frames per pixel reported in Figure 4, and in which the star PSF is subtracted perfectly, i.e., only leaving detector and photon noise after subtraction. This condition represents the theoretical detection limit, and clearly demonstrates how the SFADI method is able to reach a residual level as low as three times the photon limit.

3.3.1. Dependence on Frame Exposure

Such high performance of the SFADI method, which relies on the very short exposure time (1 ms) of the single frames of our data set, would not be possible with longer integration times, as the speckle pattern has a typical lifetime of the order of a few milliseconds (Stangalini et al. 2017), as we mentioned in Section 3.1.

In order to better illustrate the SFADI performance with respect to the frame exposure time, we simulated longer integration times by summing up together 4, 16, and 64 sequential frames and applying the SWAMIS identification code to them, as displayed in Figure 6. As the frame integration increases, the quality of speckle recognition decreases. This is because multiple speckles are merged together.

Figure 7 quantitatively shows the increment in background artifacts for the 4 ms and 16 ms cases and how the 2×10^{-5} planets become undetectable, with respect to the 1 ms case in the second panel of Figure 5. This demonstrates that a KHz frame rate is mandatory for boosting the SFADI to its maximum performance.

3.3.2. Dependence on the Number of Frames

We finally compared the SFADI and ADI behavior as a function of the number of images in the frames sequence, in order to clarify whether acquiring a longer sequence effectively increases the quality of the result.

This is not obvious, because in the presence of highly variable seeing conditions, like in our data set, the difference between the estimated PSF and the instantaneous PSF increases with the number of frames.

For this reason, even if the detector and photon noise percentage contribution decreases by increasing the acquisition time, the residuals of the standard ADI do not decrease. In fact, in the case of our data set the seeing regime was different for different intervals of the observation, so that the ADI residuals increase as the image sequence gets longer (see Figure 8).

On the contrary, the SFADI method is not sensitive to the seeing variation, because the instantaneous PSF is canceled out by speckle masking in each frame. Consequently, the standard deviation of background residuals keeps reducing with time as depicted by the blue line in Figure 8.

3.4. Extended Sources and Fast Acquisitions: From SFADI to SFI

The speckle suppression technique that we described is not only useful for detecting point sources like extra-solar planets, binary stars, or background stellar objects, but it also opens the possibility of performing high-contrast imaging on extended sources, such as circumstellar disks and jets or AGN structures, and around multiple bright stars.

The main obstacle for the observation of extended features with standard ADI is that, if the size of the feature is not significantly smaller than the arc subtended by field rotation at the feature's position, the median PSF model contains an angularly smoothed ghost of the feature itself, thus leading to self-subtraction in the final residual. The same also happens for planets when the frame sequence is not long enough to locate the planet in the last frames at a sufficiently different position angle from the first frames.

On the contrary, if the speckles are masked, as we do in the SFADI, the remaining background virtually contains no starlight, but only light from the astronomical source of interest, so that we can skip the stage of median PSF subtraction and directly combine the de-rotated masked frames, revealing the extended feature in the background. In this case, we skip any angular differential operations, so that we simply call this procedure "SFI," for "Speckle-Free Imaging."

As an example of this procedure, we simulated the observation of a binary star surrounded by extended circumstellar structures, which we report in Figure 9. The image model that we have considered (first panel in Figure 9) was built from the deconvolved image of the young binary Z CMa obtained by Antoniucci et al. (2016) using [O I] λ6300 line SPHERE/ZIMPOL observations, scaled to the same flux of the SHARK-VIS Forerunner target star. In the circumstellar structure, we can identify a wide-angle stellar wind emitted by the NW component (labeled with W) and a collimated jet driven by SW component (labeled with J), whose fluxes are

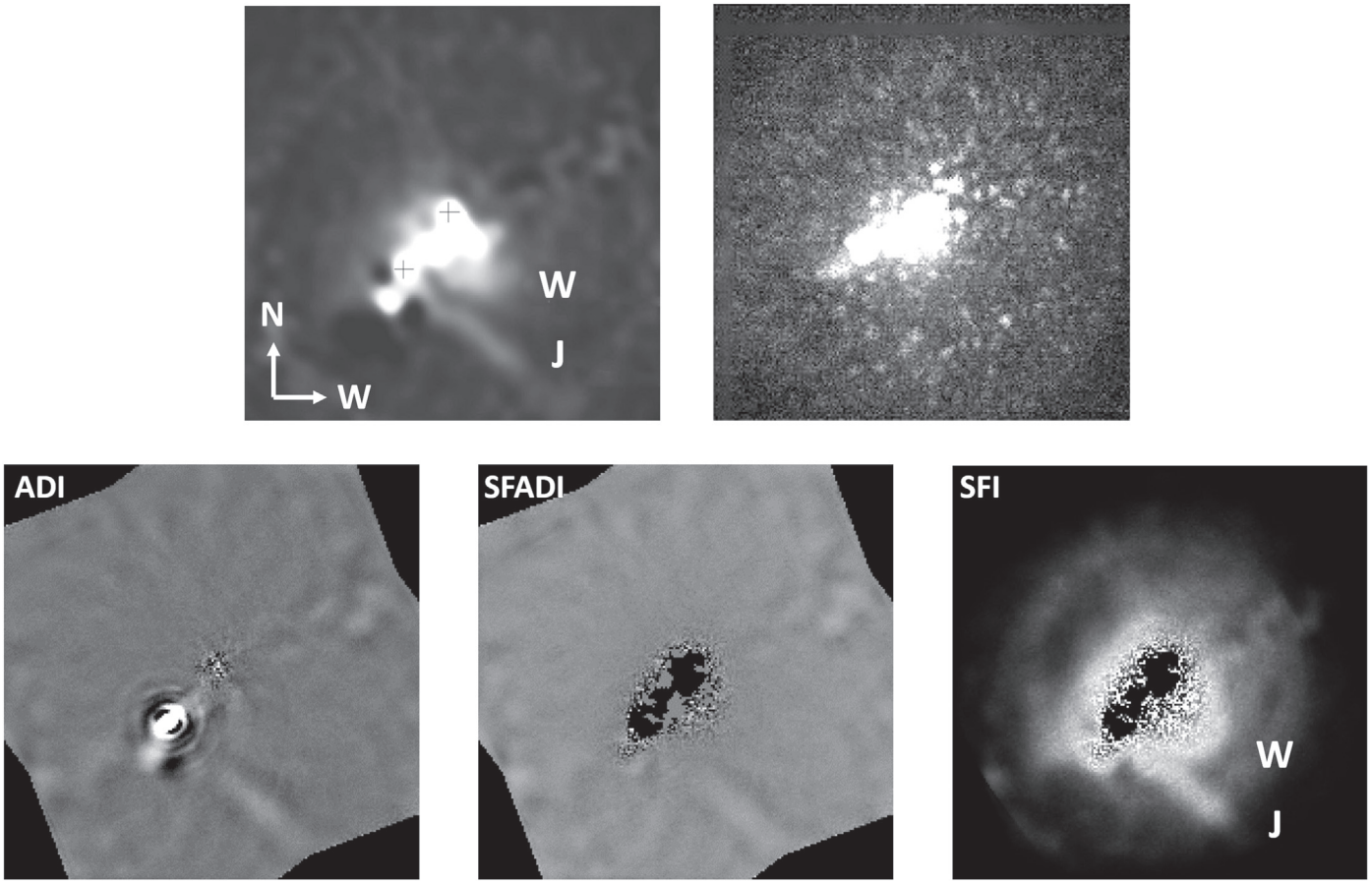

Figure 9. Extended circumstellar structure (10^{-4} contrast) around the ZCMa binary (whose flux-scaled model, based on Antoniucci et al. 2016, is shown in the top-left panel) as viewed after convolution with the PSF of a single frame of the SHARK-VIS Forerunner sequence (top-right). In the bottom panels, the results of the application of ADI, SFADI, and SFI methods are shown (from left to right, respectively). The W and J labels indicate the wide wind from the primary NW component, and the collimated jet from the secondary star, respectively.

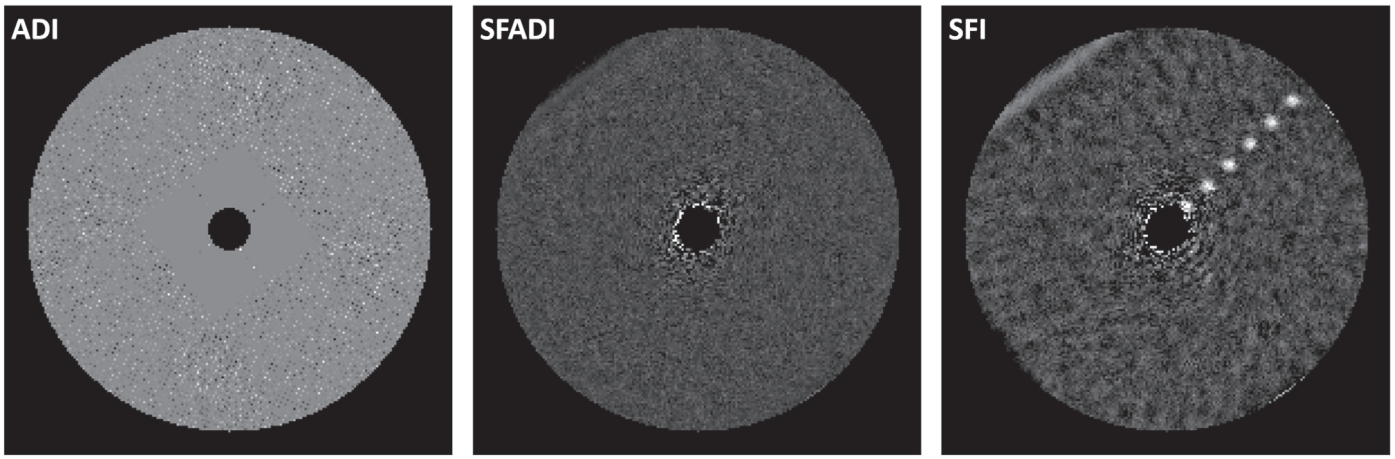

Figure 10. Simulation of six 5×10^{-4} contrast planets, from 50 to 300 mas separation, with 5 s acquisition after ADI, SFADI, and SFI post-processing methods (from left to right respectively). Note the visibility of the inner planet at only 50 mas of separation from the central star.

scaled to an average contrast of about 10^{-4} with respect to the brightest NW component.

Both components of this binary produce speckles in each frame of the sequence (second panel in Figure 9) and both speckle systems are identified by the SWAMIS speckle mask. The result, as the lower panels clearly show, is that both the W and J extended structures are well imaged by the SFI technique (last panel), while the ADI and the SFADI contain strong artifacts by self-subtracted image components.

Finally, Figure 10 depicts the case of a very short acquisition sequence lasting 5 s only, which does not provide enough field rotation to disentangle the simulated 5×10^{-4} contrast planets, which in fact are not recovered by either ADI (left) and SFADI (center), but which are well detected by the SFI method (right).

This means that the SFI technique can also be used to have a real-time preview of the SFADI result just after the very first frames of a long acquisition sequence.

4. Conclusions

We introduced the new Speckle-Free Angular Differential Imaging (SFADI) technique for high-contrast imaging, based on speckle identification and masking on millisecond cadence acquisitions.

The presented method substantially improves the standard ADI performances for both planet detection and extended sources nearby single-conjugated adaptive optics guide stars.

Applying SFADI to a real 20-minute sequence of 1 ms exposure frames acquired at LBT, for which the standard ADI contrast limit is 5×10^{-5} at 100 mas, we reach a contrast limit of 1×10^{-5} despite the poor and highly variable seeing conditions (0.8 to 1.5 arcsec) of the observation.

We also presented extended tests to characterize how the SFADI results depend on the frame integration time and on the number of acquired frames. We show that, thanks to the fast KHz frame rate, the SFADI performances approach the theoretical photon limit, and that they continue improving as the acquisition time increases, suggesting that very high-contrast limits can be reached with long observations.

At last, we introduce the Speckle-Free Imaging (SFI) technique, which is based on the SFADI concept and opens high-contrast imaging to extended objects and to fast acquisitions.

This study has been supported by the ADONI Italian National Laboratory for Adaptive Optics and developed to fully exploit the performances of the SHARK-VIS high-contrast imager for LBT, currently under construction.

The LBT is an international collaboration among institutions in the United States, Italy, and Germany. LBT Corporation partners are The University of Arizona on behalf of the Arizona Board of Regents; Istituto Nazionale di Astrofisica, Italy; LBT Beteiligungsgesellschaft, Germany, representing the Max-Planck Society, the Leibniz Institute for Astrophysics Potsdam, and Heidelberg University; and The Ohio State University, and The Research Corporation, on behalf of The University of Notre Dame, University of Minnesota and University of Virginia.

Facility: LBT.

Software: SWAMIS (DeForest et al. 2007).

ORCID iDs

Gianluca Li Causi https://orcid.org/0000-0001-9539-2112
Marco Stangalini https://orcid.org/0000-0002-5365-7546
Simone Antoniucci https://orcid.org/0000-0002-0666-3847
Fernando Pedichini https://orcid.org/0000-0002-0983-8040
Vincenzo Testa https://orcid.org/0000-0003-1033-1340

References

Amara, A., & Quanz, S. P. 2012, MNRAS, 427, 948
Antoniucci, S., Podio, L., Nisini, B., et al. 2016, A&A, 593, L13
Bailey, V. P., Hinz, P. M., Puglisi, A. T., et al. 2014, Proc. SPIE, 9148, 914803
Beuzit, J.-L., Feldt, M., Dohlen, K., et al. 2006, Msngr, 125, 29
Bonnefoy, M. 2015, AAS meeting, 203.05
Cavarroc, C., Boccaletti, A., Baudoz, P., Fusco, T., & Rouan, D. 2006, A&A, 447, 397
Close, L. M., Follette, K., Males, J. R., et al. 2014, in IAU Symp. 299, Exploring the Formation and Evolution of Planetary Systems, ed. M. Booth, B. C. Matthews, & J. R. Graham (Cambridge: Cambridge Univ. Press), 32
Currie, T. 2015, AAS meeting, 203.04
Davies, R., & Kasper, M. 2012, ARA&A, 50, 305
DeForest, C. E., Hagenaar, H. J., Lamb, D. A., Parnell, C. E., & Welsch, B. T. 2007, ApJ, 666, 576
Esposito, S., Riccardi, A., Fini, L., et al. 2010, Proc. SPIE, 7736, 773609
Hardy, A., Schreiber, M. R., Parsons, S. G., et al. 2015, ApJL, 800, L24
Jefferies, S. M., & Hart, M. 2011, OExpr, 19, 1975
Kasper, M. 2012, Proc. SPIE, 8447, 84470B
Labeyrie, A. 1995, A&A, 289, 544
Lafrenière, D., Marois, C., Doyon, R., Nadeau, D., & Artigau, É 2007, ApJ, 660, 770
Lamb, D. A., DeForest, C. E., Hagenaar, H. J., Parnell, C. E., & Welsch, B. T. 2008, ApJ, 674, 520
Lamb, D. A., DeForest, C. E., Hagenaar, H. J., Parnell, C. E., & Welsch, B. T. 2010, ApJ, 720, 1405
Lamb, D. A., Howard, T. A., DeForest, C. E., Parnell, C. E., & Welsch, B. T. 2013, ApJ, 774, 127
Macintosh, B., Graham, J. R., Ingraham, P., et al. 2014, PNAS, 111, 12661
Macintosh, B. A., Graham, J. R., Palmer, D. W., et al. 2008, Proc. SPIE, 7015, 701518
Males, J. R., Close, L. M., Morzinski, K. M., et al. 2014a, in IAU Symp. 299, Exploring the Formation and Evolution of Planetary Systems, ed. M. Booth, B. C. Matthews, & J. R. Graham (Cambridge: Cambridge Univ. Press), 46
Males, J. R., Close, L. M., Morzinski, K. M., et al. 2014b, ApJ, 786, 32
Marois, C., Lafrenière, D., Doyon, R., Macintosh, B., & Nadeau, D. 2006, ApJ, 641, 556
Pedichini, F., Stangalini, M., Ambrosino, A., et al. 2017, AJ, 154, 74
Soummer, R., Pueyo, L., & Larkin, J. 2012, ApJL, 755, L28
Stangalini, M. 2014, A&A, 561, L6
Stangalini, M., Giannattasio, F., & Jafarzadeh, S. 2015, A&A, 577, A17
Stangalini, M., Pedichini, F., Pinna, E., et al. 2017, JATIS, 3, 025001